Physics in Medicine & Biology

IPEM
Institute of Physics and Engineering in Medicine

PAPER

Consideration of the effects of intense tissue heating on the RF electromagnetic fields during MRI: simulations for MRgFUS in the hip

To cite this article: Sherman Xuegang Xin *et al* 2015 *Phys. Med. Biol.* **60** 301

IOP Publishing | Institute of Physics and Engineering in Medicine Physics in Medicine & Biology

Phys. Med. Biol. **60** (2015) 301–307 doi:10.1088/0031-9155/60/1/301

Consideration of the effects of intense tissue heating on the RF electromagnetic fields during MRI: simulations for MRgFUS in the hip

Sherman Xuegang Xin[1,2,3], Shiyong Gu[1], Giuseppe Carluccio[2] and Christopher M Collins[2]

[1] Biomedical Engineering School of the Southern Medical University, Guangzhou city, 510515 People's Republic of China
[2] Bernard and Irene Schwartz Center for Biomedical Imaging, New York University School of Medicine, New York, NY 10016, USA

E-mail: shermansheen@gmail.com

Received 23 May 2014, revised 15 October 2014
Accepted for publication 19 November 2014
Published 12 December 2014

Abstract

Due to the strong dependence of tissue electrical properties on temperature, it is important to consider the potential effects of intense tissue heating on the RF electromagnetic fields during MRI, as can occur in MR-guided focused ultrasound surgery. In principle, changes of the RF electromagnetic fields could affect both efficacy of RF pulses, and the MRI-induced RF heating (SAR) pattern. In this study, the equilibrium temperature distribution in a whole-body model with 2 mm resolution before and during intense tissue heating up to 60 °C at the target region was calculated. Temperature-dependent electric properties of tissues were assigned to the model to establish a temperature-dependent electromagnetic whole-body model in a 3T MRI system. The results showed maximum changes in conductivity, permittivity, $\left|\mathbf{B}_1^+\right|$, and SAR of about 25%, 6%, 2%, and 20%, respectively. Though the B_1 field and SAR distributions are both temperature-dependent, the potential harm to patients due to higher SARs is expected to be minimal and the effects on the B_1 field distribution should have minimal effect on images from basic MRI sequences.

Keywords: temperature-dependent electric properties, magnetic resonance imaging (MRI), radiofrequency (RF) electromagnetic fields, specific absorption rate (SAR)

(Some figures may appear in colour only in the online journal)

[3] Author to whom correspondence should be addressed.

1. Introduction

With magnetic resonance imaging (MRI) it is possible to map temperature change *in vivo* non-invasively (Rieke and Butts Pauly 2008). MRI-guided focused ultrasound surgery (MRgFUS) is a relatively new technology (Bradley 2009), used for the thermal ablation of uterine fibroid, pancreas tumors, etc (Jenne *et al* 2012), or used for the palliative treatment of painful bone metastases (Gianfelice *et al* 2008). In this technique, MRI and MR thermography can guide and monitor focused ultrasound thermal surgery to ensure that temperature is safely controlled. Based on a recent study of the measurement of dielectric properties of biological tissues, electrical conductivity of some tissues could change more than 20% during the process of MRgFUS (Fu *et al* 2014). Due to the strong dependence of tissue electrical properties on temperature (Lazebnik *et al* 2006, Zurbuchen *et al* 2010), it is important to consider the potential effects of intense tissue heating on the RF electromagnetic fields during MRI, as can occur in MRgFUS. Changes of the RF electromagnetic fields resulting from the changes in tissue electrical properties during an MR scan may affect, for example, both the efficacy of RF pulses and the MRI-induced specific absorption rate (SAR) pattern (Collins and Wang 2011). To the best of our knowledge, however, a study of the potential effects of intense tissue heating on the RF electromagnetic fields during MRI has not previously been performed.

In this study, an equilibrium temperature distribution inside a body model with a resolution of 2 mm was calculated as may occur in focused ultrasonic heating for palliative care of patients with bone metastases (Gianfelice *et al* 2008). Simulations of RF electromagnetic fields in the body model before and during intense focal tissue heating related to thermal ablation were then performed. Temperature-induced changes of the distribution of RF electromagnetic fields and SAR in MRI are presented and discussed.

2. Methods

In this work, the temperature distribution in a whole-body model with 2 mm resolution during MRgFUS therapy was first calculated using a previously published algorithm (Collins *et al* 2004). Then the temperature-dependent dielectric properties of tissues were assigned to the whole-body model according to the calculated temperature distribution to establish a temperature-dependent electromagnetic whole body model. Finally, numerical simulations were performed to determine the changes of RF electromagnetic fields due to the intense tissue heating. These steps are described in further detail below.

A temperature distribution map from MRgFUS designed for pain palliation in a patient with iliac bone metastases was simulated using a 2 mm numerical model of the human body, NAOMI (Dimbylow 1997, 1998), by defining a focal region in the iliac bone where the temperature was fixed at 60 °C (Gianfelice *et al* 2008). The focal region was spherical, with a diameter of 75 mm, and included only cortical bone. The equilibrium temperature distribution throughout the rest of body was calculated using a self-convergent iterative algorithm which considers thermal conduction, blood perfusion, and other relevant factors (Collins *et al* 2004). The algorithm uses a finite difference implementation of the Pennes bioheat equation (Pennes 1948):

$$\rho C\left(\frac{\mathrm{d}T}{\mathrm{d}t}\right) = \nabla \cdot (k \nabla T) + \left[-\rho_{\mathrm{blood}} W C_{\mathrm{blood}} (T - T_{\mathrm{core}})\right] + Q_m \tag{1}$$

where ρ is the material density, C is the heat capacity, k is the thermal conductivity, W is the perfusion by blood, Q_m is the heat generated by metabolism. All the values of the above parameters and other details of the algorithm were obtained from the literature (Collins *et al* 2004).

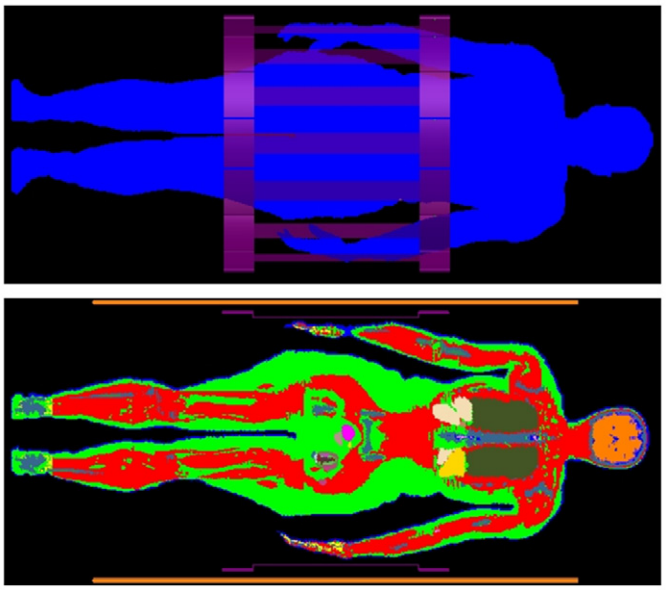

Figure 1. Top: 3D rendering of the whole-body 3D model with 2 mm resolution loaded in birdcage coil. Bottom: coronal slice chosen to show a variety of internal tissues.

After finishing the calculation of the equilibrium temperature distribution with and without the region of focal heating, recently-measured tissue-specific temperature-dependent electric properties in agreement with published values were assigned to the voxels of the body model in the region of high temperature to create a second model with electrical property distribution as could be expected in the high-temperature state (Fu *et al* 2014). The temperature-dependent dielectric properties of three tissues, muscle, fat, and bone, were needed in this study. While the temperature dependent dielectric properties of muscle and fat at 128 MHz have been reported (Fu *et al* 2014), data for bone at this frequency is not currently available from the literature. Because cortical bone has low water content, it (like fat) is expected to have relatively low electric permittivity and conductivity at any frequency or temperature, and thus its variation should have relatively little effect on the RF field distribution. In this work the temperature-dependent dielectric properties of bone were assigned those of fat. A 16-rung, low-pass birdcage coil with a diameter of 60 cm and a height of 40 cm loaded with the modified whole body model at 128 MHz (3 T) was used in the simulation (figure 1). The finite difference time domain (FDTD) method for electromagnetics (Kane 1966) was used to determine the steady-state RF electromagnetic field distributions. The spatial resolution of the calculation region was 2 mm in all three directions. All FDTD calculations were performed using commercial software (XFDTD; Remcom, Inc.; State College, PA) (Trakic *et al* 2004).

The circularly polarized RF transmit magnetic field $\mathbf{B}_1^+$, was calculated as (Hoult 2000)

$$\mathbf{B}_1^+ = \frac{1}{2}\left(\widetilde{\mathbf{B}}_\mathbf{x} + \mathrm{i}\widetilde{\mathbf{B}}_\mathbf{y}\right) \tag{2}$$

where $\widetilde{\mathbf{B}}_\mathbf{x}$ and $\widetilde{\mathbf{B}}_\mathbf{y}$ are the complex magnetic flux density of RF electromagnetic field along orthogonal directions in the transverse plane as obtained from the FDTD calculation. SAR_n was calculated at every location in the model as (Collins and Smith 2001)

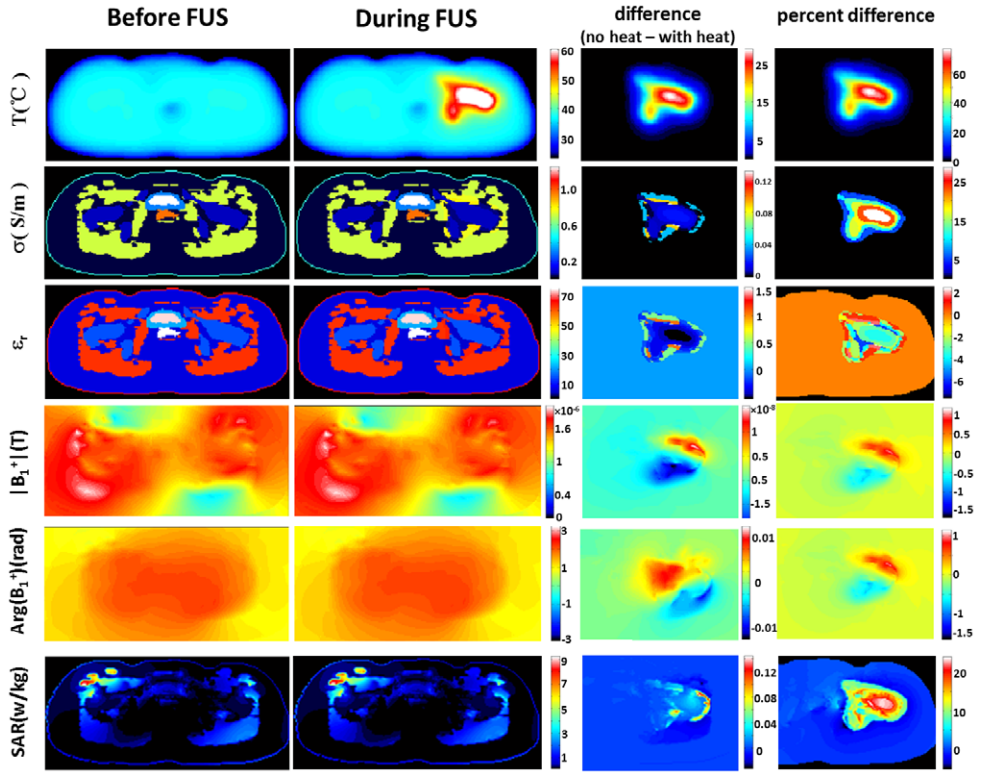

Figure 2. Comparison of temperature, conductivity, relative permittivity, amplitude of $\mathbf{B}_1^+$, phase of $\mathbf{B}_1^+$, and SAR before and during heating. The distribution, the absolute difference, and the percent of difference of these parameters are shown on a transverse plane passing through the middle of the region of maximum temperature increase.

$$\mathrm{SAR}_n = \frac{\sigma}{2\rho_n}\left(|\mathbf{E}_x|^2 + |\mathbf{E}_y|^2 + |\mathbf{E}_z|^2\right) \tag{3}$$

where $\mathbf{E}$, σ, and ρ refer to the RF electric field, tissue conductivity, and density, respectively. The subscript n indicates the voxel in the simulation region.

A gradient echo MR image was simulated by multiplying the amplitude of $\mathbf{B}_1^+$ by a value roughly proportional to tissue proton density content. This method assumes that a low excitation flip angle, a reconstruction method which removes the weighting of the RF receive coil distribution (Pruessmann *et al* 1999), and an effective method of fat suppression are used. Compared to an excitation flip angle near 90°, this will accentuate effects of $\mathbf{B}_1^+$ inhomogeneity on the simulated image.

3. Results and discussion

The comparison of temperature, conductivity, relative permittivity, $|\mathbf{B}_1^+|$, and SAR before and after heating is shown in figure 2. A temperature gradient distribution after equilibrium was established inside the body centered at the region of interest, extending into the surrounding muscle and fat tissues. The difference in temperature between the state with and without the

Figure 3. Simulated proton density weighted gradient echo images before and during focal heating, and the percent difference between them.

ultrasonic heating was as high as 23 °C, and the percent of temperature difference on the Celsius scale was more than 60% (figure 2). The maximum change in conductivity was more than 25%, while that in permittivity was only about 6%. The maximum change in $\left|\mathbf{B}_1^+\right|$ was less than 2%, and that in the phase of the $\mathbf{B}_1^+$ field was less than 6°, indicating that only minor influence of the temperature-dependence of the $\mathbf{B}_1^+$ field. The maximum relative change of SAR was about 20%. This occurred in the defined focal region, as indicated in figure 2. In this case the region of ultrasonic heating (also the region of maximum change in SAR) was not near the region of maximum local SAR, and had no effect on this measure of RF safety. Even in the event that the region of ultrasonic heating would coincide with that of maximum local SAR, it is expected that maximal MR-induced heating (on the order of 1 °C) would be a small fraction of that due to the ultrasonic heating and would likely not be a major consideration for MR safety.

Simulated images from before and after ultrasonic heating are shown in figure 3. As expected from the minimal changes in $\mathbf{B}_1{}^+$ alone, the effects on image intensity due to temperature-dependent tissue electrical properties are very small. It is important to note, however, that this analysis, assuming a strongly proton density weighted image, does not consider effects of temperature on T_1 and T_2 that may affect signal intensity in images from other sequences. The effects of heating on the phase of the $\mathbf{B}_1{}^+$ field should also have only a small effect on the accuracy of conventional phase-based MR thermography. For example, assuming a proton resonance shift based method of MR thermography (Reike and Butts Pauly 2008) with a temperature-dependent chemical shift coefficient of −0.01 ppm and a gradient-echo sequence with a TR of about 20 ms, a temperature increase of 20 °C should result in a change in phase of a little more than 180°. Thus the temperature-induced changes in the RF fields of about 6° could produce about an error of about 3% (or 0.6° for the assumed 20 °C change), which is close to the uncertainty of *in vivo* MR thermography itself at 3 T. The size of this relative error would be inversely proportional to the length of TE chosen for the MR thermography sequence.

This work represents an initial study into the potential effects of intense tissue heating on the RF fields and SAR in MRI, and was performed on a single model of a single human subject. Though the $\mathbf{B}_1^+$ field and SAR distribution may vary with different human bodies having different morphologies (Liu *et al* 2005), the scale of temperature dependence should be similar. The temperature changes studied here, ranging to about 30 °C, may not cover the range for all treatment paradigms. Further study including a larger range would also require characterization of the temperature-dependence of tissue dielectric properties at MR frequencies over a larger range than is currently available. Also, while different MR sequences may produce $\mathbf{B}_1^+$ field and SAR with different amplitudes, the distribution patterns will not change such that the alterations of $\mathbf{B}_1^+$ field and SAR in percentage before and after heating will be the same for any MR sequence.

This study does not consider the potential effect of cavitation bubbles, which may be produced by high intensity ultrasound pules as another treatment strategy. Exploration of the possible impact of cavitation on the $\mathbf{B}_1^+$ field and SAR in MRI would require further study and development of different model.

In thermal ablation, some thermally-induced physiological changes, such as those in blood perfusion or due to coagulation, will result in alterations of local volume magnetic susceptibility of tissues (Sprinkhuizen *et al* 2012). Effects of susceptibility on the $\mathbf{B}_1^+$ field are only on the order of a few parts per million (ppm), and are negligible compared to the changes shown here (de Lacheisserie *et al* 2005). However, the alterations of the static magnetic (B_0) field of the order of ppm due to the change of local volume susceptibility of tissues cannot be neglected. The impact of temperature-dependent volume susceptibility on MR thermometry has been noticed and reported (Sprinkhuizen *et al* 2010).

Usually there are no metal parts of the ultrasound probes that could contact with or be inside the human tissues during the MRgFUS process. In rare cases, the MRgFUS surgery could be performed in patients who were already implanted metallic devices. MR imaging of patients with implanted metallic devices can result in very different SAR distributions than seen here (Mattei *et al* 2008), and is beyond the scope of this work. In the absence of implants and for lower temperature increases, field and temperature simulations like those seen here are seen to be in reasonably good agreement with measurement in phantoms and *in vivo* (Oh *et al* 2014).

4. Conclusion

Results show that the B_1 field and SAR distributions are both temperature-dependent. The potential harm to patients due to higher SAR is expected to be minimal in a situation such as MRgFUS, where temperature increase is dominated not by the RF fields of the MR system, but by the energy from the intense focused ultrasound system. The effects on the B_1 field distribution should have minimal localized effect on images and even MR thermometry measurements acquired with commonly used MRI sequences.

Acknowledgments

This study was partially supported by the National Natural Science Foundation of China (grant number 61172034), Science and Technology Program of Guangzhou, China (no. 2014J4100160), and the National Institute of Health (grant numbers NIH R01 EB000454 and NIH R01EB011551). The authors report no conflicts of interests.

References

Bradley W G Jr 2009 MR-guided focused ultrasound: a potentially disruptive technology *J. Am. College Radiol.: JACR* **6** 510–3

Collins C M, Liu W Z, Wang J H, Gruetter R, Vaughan J T, Ugurbil K and Smith M B 2004 Temperature and SAR calculations for a human head within volume and surface coils at 64 and 300 MHz *J. Magn. Reson. Imaging* **19** 650–6

Collins C M and Smith M B 2001 Signal-to-noise ratio and absorbed power as functions of main magnetic field strength, and definition of '90°' RF pulse for the head in the birdcage coil *Magn. Reson. Med.* **45** 684–91

Collins C M and Wang Z 2011 Calculation of radiofrequency electromagnetic fields and their effects in MRI of human subjects *Magn. Reson. Med.* **65** 1470–82

de Lacheisserie E T, Gignoux D and Schlenker M 2005 *Magnetism: Materials and Applications* vol 2 (New York: Springer)

Dimbylow P J 1997 FDTD calculations of the whole-body averaged SAR in an anatomically realistic voxel model of the human body from 1 MHz to 1 GHz *Phys. Med. Biol.* **42** 479–90

Dimbylow P J 1998 Induced current densities from low-frequency magnetic fields in a 2 mm resolution, anatomically realistic model of the body *Phys. Med. Biol.* **43** 221–30

Fu F R, Xin S X and Chen W F 2014 Temperature- and frequency-dependent dielectric properties of biological tissues within the temperature and frequency ranges typically used for magnetic resonance imaging-guided focused ultrasound surgery *Int. J. Hyperthermia* **30** 56–65

Gianfelice D, Gupta C, Kucharczyk W, Bret P, Havill D and Clemons M 2008 Palliative treatment of painful bone metastases with MR imaging—guided focused ultrasound *Radiology* **249** 355–63

Hoult D I 2000 The principle of reciprocity in signal strength calculations—a mathematical guide *Concept Magn. Res.* **12** 173–87

Jenne J W, Preusser T and Gunther M 2012 High-intensity focused ultrasound: principles, therapy guidance, simulations and applications *Zeitschrift fur medizinische Physik* **22** 311–22

Kane Y 1966 Numerical solution of initial boundary value problems involving maxwell's equations in isotropic media *IEEE Trans. Antennas Propag.* **14** 302–7

Lazebnik M, Converse M C, Booske J H and Hagness S C 2006 Ultrawideband temperature-dependent dielectric properties of animal liver tissue in the microwave frequency range *Phys. Med. Biol.* **51** 1941–55

Liu W, Collins C M and Smith M B 2005 Calculations of B1 distribution, specific energy absorption rate, and intrinsic signal-to-noise ratio for a body-size birdcage coil loaded with different human subjects at 64 and 128 MHz *Appl. Magn. Reson.* **29** 5–18

Mattei E, Triventi M, Calcagnini G, Censi F, Kainz W, Mendoza G, Bassen H I and Bartolini P 2008 Complexity of MRI induced heating on metallic leads: experimental measurements of 374 configurations *Biomed. Eng. Online* **7** 11

Oh S, Ryu Y-C, Carluccio G, Sica C T and Collins C M 2014 Measurement of SAR-induced temperature increase in a phantom and *in vivo* with comparison to numerical simulation *Magn. Reson. Med.* **71** 1923–31

Pennes H H 1948 Analysis of tissue and arterial blood temperatures in the resting human forearm *J. Appl. Physiol.* **1** 93–122

Pruessmann K P, Weiger M, Scheidegger M B and Boesiger P 1999 SENSE: sensitivity encoding for fast MRI *Magn. Reson. Med.* **42** 952–62

Rieke V and Butts Pauly K 2008 MR thermometry *J. Magn. Reson. Imaging* **27** 376–90

Sprinkhuizen S M, Bakker C J, Ippel J H, Boelens R, Viergever M A and Bartels L W 2012 Temperature dependence of the magnetic volume susceptibility of human breast fat tissue: an NMR study *Magn. Reson. Mater. Phys. Biol. Med.* **25** 33–9

Sprinkhuizen S M, Konings M K, van der Bom M J, Viergever M A, Bakker C J and Bartels L W 2010 Temperature-induced tissue susceptibility changes lead to significant temperature errors in PRFS-based MR thermometry during thermal interventions *Magn. Reson. Med.* **64** 1360–72

Trakic A, Crozier S and Liu F 2004 Numerical modelling of thermal effects in rats due to high-field magnetic resonance imaging (0.5–1 GHz) *Phys. Med. Biol.* **49** 5547

Zurbuchen U, Holmer C, Lehmann K S, Stein T, Roggan A, Seifarth C, Buhr H J and Ritz J P 2010 Determination of the temperature-dependent electric conductivity of liver tissue *ex vivo* and *in vivo*: importance for therapy planning for the radiofrequency ablation of liver tumours *Int. J. Hyperthermia* **26** 26–33